BASIC SCIENCE

Nanomedicine: Nanotechnology, Biology, and Medicine
48 (2023) 102650

Feature Article

nanomedjournal.com

Dye labeling for optical imaging biases drug carriers' biodistribution and tumor uptake

Sarah Schraven, MSc[a], Stefanie Rosenhain, PhD[a,b], Ramona Brueck[a], Tim Marvin Wiechmann, MSc[a], Robert Pola, PhD[c], Tomáš Etrych, PhD[c], Wiltrud Lederle, DSc[a], Twan Lammers, PhD[a], Felix Gremse, PhD[a,b], Fabian Kiessling, MD[a,d,e,*]

[a]*Institute for Experimental Molecular Imaging, RWTH Aachen University, Forckenbeckstrasse 55, 52074 Aachen, Germany*
[b]*Gremse-IT GmbH, Dennewartstrasse 25, 52068 Aachen, Germany*
[c]*Institute of Macromolecular Chemistry, Czech Academy of Sciences, Heyrovského nám. 2, 162 06 Prague, Czech Republic*
[d]*Helmholtz Institute for Biomedical Engineering, RWTH Aachen University, Aachen, Germany*
[e]*Fraunhofer MEVIS, Institute for Medical Image Computing, Aachen, Germany*

Revised 25 December 2022

Abstract

Biodistribution analyses of nanocarriers are often performed with optical imaging. Though dye tags can interact with transporters, e.g., organic anion transporting polypeptides (OATPs), their influence on biodistribution was hardly studied. Therefore, this study compared tumor cell uptake and biodistribution (in A431 tumor-bearing mice) of four near-infrared fluorescent dyes (AF750, IRDye750, Cy7, DY-750) and dye-labeled poly(*N*-(2-hydroxypropyl)methacrylamide)-based nanocarriers (dye-pHPMAs). Tumor cell uptake of hydrophobic dyes (Cy7, DY-750) was higher than that of hydrophilic dyes (AF750, IRDye750), and was actively mediated but not related to OATPs. Free dyes' elimination depended on their hydrophobicity, and tumor uptake correlated with blood circulation times. Dye-pHPMAs circulated longer and accumulated stronger in tumors than free dyes. Dye labeling significantly influenced nanocarriers' tumor accumulation and biodistribution. Therefore, low-interference dyes and further exploration of dye tags are required to achieve the most unbiased results possible. In our assessment, AF750 and IRDye750 best qualified for labeling hydrophilic nanocarriers.

Keywords: Molecular imaging; Optical imaging; Fluorescent dye-labeling; Drug delivery system; Biodistribution

Data availability: Data will be made available on request.

Background

Non-invasive imaging is frequently applied in drug development and basic research to assess the biodistribution of drugs and biomolecules, which are often labeled radioactively for tracking by positron emission tomography (PET) or single-photon emission computed tomography (SPECT).[1,2] Although PET and SPECT are widely accepted and quantitative, the throughput of animals is limited, and costs are high due to the complexity of generating the radiolabeled probes and handling of radioactive animals. The decay times of the radiolabeled probes pose further organizational challenges to larger animal trials. High safety precautions must be implemented due to exposure of personnel and animals to radiation.

An alternative is optical imaging with fluorescent probes, which is considered safe, less costly, and capable of higher throughput rates. However, quantifying fluorescence imaging data is difficult due to strong absorption and scattering of light in organisms. Therefore, classical 2D reflectance imaging approaches can hardly be applied for biodistribution studies. This limitation has been overcome by hybrid computed tomography-fluorescence tomography (CT-FLT), a 3D technology that

Funding: This work was supported by the Deutsche Forschungsgemeinschaft (German Research Foundation) [grant numbers 403224013, 331065168], and the Czech Science Foundation [grant number 22-12483S].
* Corresponding author at: Institute for Experimental Molecular Imaging, RWTH Aachen University, Aachen, Germany.
E-mail address: fkiessling@ukaachen.de (F. Kiessling).

https://doi.org/10.1016/j.nano.2023.102650
1549-9634/

Please cite this article as: Schraven S, et al, Dye labeling for optical imaging biases drug carriers' biodistribution and tumor uptake. *Nanomedicine: NBM* 2023;48:102650, https://doi.org/10.1016/j.nano.2023.102650

models the diffuse light scattering after pointwise illumination.[3,4] The accuracy of CT-FLT was highlighted by directly comparing hybrid PET-magnetic resonance imaging with CT-FLT regarding biodistribution data of different antibody formats in mice.[5] Another study demonstrated that fluorescent dyes can be detected and quantified in deep tissue regions of mice in picomolar concentrations.[6]

However, changing a single functional group of a molecule can influence its biodistribution. This is even more true for imaging tags like radionuclide chelators or the considerably larger fluorescent dyes. For the latter, even for macromolecules, pronounced changes in the biodistribution were described.[5,7,8] The observed changes will depend on the dyes' structure, polarity, type of labeling, and interaction with endogenous biomolecules.[9] It has even been hypothesized that dye-labeled probes are actively taken up by transporters, such as organic anion transporting polypeptides (OATPs).[5,10,11] Furthermore, hydrophobicity and albumin binding affinity can affect biodistribution, tumor uptake, and clearance.[12,13] Besides this, dyes can also modify the macromolecular structure of the labeled moiety itself, e.g., protein folding could change due to charge alterations.[12]

Despite these limitations, CT-FLT has a high complementary value to PET and SPECT for biodistribution studies and thus, may become a standard tool in drug development. However, to obtain reliable results and draw the right conclusions from CT-FLT data, knowledge about the influence of dyes on the biodistribution of labeled probes is essential. Thus, for biodistribution analyses it is of great interest to identify low interfering dyes. Therefore, we systematically assessed cell uptake and biodistribution of four commonly applied near-infrared fluorescent (NIRF) dyes and investigated their influence on uptake and biodistribution of a model drug delivery system (DDS).

Methods

Synthesis and conjugation of the DDS

The model DDS poly(*N*-(2-hydroxypropyl)methacrylamide)-*co*-aminoethyl-methacrylate copolymer (pHPMA-co-AEMA, for simplicity abbreviated to pHPMA here) was synthesized by reversible addition-fragmentation chain-transfer polymerization. The N-hydroxysuccinimide esters of AF750 (Thermo Fisher Scientific, Waltham, MA, USA), IRDye750 (LI-COR, Lincoln, NE, USA), Cy7 (Lumiprobe GmbH, Hannover, Germany), and DY-750 (Dyomics GmbH, Jena, Germany) were conjugated to the polymer. A detailed overview of the synthesis of the polymer-based DDS and the conjugation can be found in the supplementary data.

Hydrophobicity of NIRF dyes

To assess the relative hydrophobicity of the dyes (DY-750, Cy7, IRDye®750-N-hydroxysuccinimide, AF750), 90 μL of a 0.4 g/L dye solution were injected into an Agilent 1269 Infinity HPLC system (Agilent, Santa Clara, CA, USA) with a reversed phase Agilent Prep-C18 Scalar column (150 × 4.6 mm) on a linear gradient of water-acetonitrile 0–100 % in presence of 0.1 % trifluoroacetic acid for 30 min and a Diode Array and Multiple Wavelength Detector.

Analysis of OATP expression

Since OATPs are believed to play a role in the uptake of fluorescent dyes, e.g., indocyanine green (ICG),[14] we first investigated OATP expression by quantitative reverse transcription polymerase chain reaction (see supplementary data).

Cellular uptake of dyes and dye-pHPMA conjugates

A431 cells, human epidermal carcinoma cells, were seeded in 24-well plates (2×10^5 cells/well). After 24 h, cells were washed trice with PBS. To investigate the cellular uptake of the dyes and the dye-pHPMAs, cells were incubated with 10 μM free dyes for 30 min or with the dye-pHPMAs (10 μM dye content on the pHPMA) for 1 h. To investigate whether the cellular uptake of free dyes was energy-dependent, free dyes were incubated for 30 min at 37 °C and 4 °C, respectively. Then, cells were washed trice with cold PBS and lysed for 30 min with 200 μL 1 % Triton X-100 on ice. 150 μL of the cell lysate was transferred to a black 96 well plate and fluorescence was assessed (730 ex/770 em) using an Infinite 200 Pro microplate reader (Tecan, Männedorf, Switzerland). To calculate concentrations (μM) of the dyes or the dye-equivalent of the dye-pHPMA conjugates, cell lysates in 1 % Triton X-100 were spiked to obtain 0.0001 μM to 0.1 μM solutions to run calibration curves. Protein concentrations (μM/μg protein) of the cell lysates were determined using the Pierce Rapid Gold BCA Protein Assay Kit (Thermo Fisher Scientific, Waltham, MA, USA) according to the manufacturers' protocol and used for normalization.

Animal experiments

Animal experiments were conducted according to German legal requirements and animal protection laws, complied with Directive 2010/63/EU, and were approved by the local authority *Landesamt für Natur, Umwelt und Verbraucherschutz* (LANUV) *Nordrhein-Westfalen*. In total 40 female athymic nude mice (Rj:ATHYM-Foxn1nu/nu, Janvier labs, Le Genest-Saint-Isle, France) were used in this study, each group including 5 mice. Tumors were induced by subcutaneous injection of 4×10^6 A431 cells in medium into the right flank of mice under isoflurane anesthesia.

In vivo biodistribution analysis of dyes and dye-pHPMA conjugates

When tumors had reached diameters of ~5 mm, the diet of mice was changed to chlorophyll-free chow (Sniff, Soest, Germany) to minimize autofluorescence (Fig. 3). Pre-scans were acquired via CT-FLT (MILabs B.V., Houten, the Netherlands) before the i.v. injection of the fluorescent probes to determine autofluorescence. Mice were monitored under isoflurane anesthesia directly after injection (<15 min), as well as 3 h, 6 h, 24 h, 48 h, 72 h, and 96 h after probe injection using CT-FLT imaging. CT scans were run in fast total body scan mode, tube voltage of 65 kV, tube current of 0.13 mA, a scan time of 1 min 32 s, and

analyzed at voxel size 0.14 × 0.14 × 0.14 mm^3. After the 96 h-scan, mice were euthanized to analyze organ fluorescence intensity ex vivo. CT and FLT scans were reconstructed by MILabs Auto Rec 1.6 and MILabs FLT Recon 1.1.0.8 (based on CT scans), respectively. Organs were segmented using Imalytics Preclinical 2.1 (Gremse-IT GmbH, Aachen, Germany) based on CT scans.[15] Blood curves were determined by segmentation of the blood-filled heart. Autofluorescence was subtracted from the fluorescence of the organ or mouse body, respectively. Total body fluorescence measured at the first time point was considered as the injected dose. Concentrations are expressed as percent injected dose/cm^3. One tumor in the DY-750-pHPMA group was not growing and therefore excluded from the analysis. One mouse died during the pre-scans due to unknown reasons. Blood half-life calculation is described in the supplementary data.

Ex vivo biodistribution analysis of the dyes and dye-pHPMA conjugates

Organs were excised and imaged by 2D fluorescence reflectance imaging (FMT5000, PerkinElmer, Waltham, MA, USA). Organs were segmented using Imalytics Preclinical 2.1 and fluorescence intensity of the organs was assessed.

Statistical analysis

Statistical analyses were performed using the GraphPad Prism 9 software (GraphPad Software, San Diego, CA, USA). Data are expressed as means ± SD with *n* replicates. Comparisons between groups for cellular uptake of dyes and dye-pHPMA conjugates, blood half-lives and tumor accumulation at 3 h, 24 h and 96 h were performed by one-way ANOVA with Holm-Šidák correction for multiple testing. For the cellular uptake of dye-pHPMA conjugates, one outlier was rejected in the AF750-pHPMA control group, based on a Grubb's test. Comparisons between the cellular uptake of free dyes at 37 °C and 4 °C, respectively, were performed using a two-way ANOVA test with Šidák multiple comparison correction. Differences were considered statistically significant for $p < 0.05$ in all statistical analyses. Pearson correlations between groups ($n = 4$) were performed after first computing the mean of the replicates and then analyzing those means.

Results

Characterization of dyes and dye-pHPMA conjugates

All four heptamethine dyes absorb and emit at similar wavelengths (Table S1). Cy7 and IRDye750 are indoline-containing cyanine dyes, while AF750 and DY-750 include both indoline and heteroaromatic groups in the backbone structure (Fig. 1A).[13] To determine relative dye hydrophobicity, reversed-phase HPLC was performed. Thus, DY-750 and Cy7, which eluted later, have a higher affinity for the column and are therefore more hydrophobic than AF750 and IRDye750 (Fig. 1C). In addition, similar conclusions on hydrophobicity can be drawn from the chemical structure and the $logD_{7.4}$ values calculated in silico (Table S1). According to the SwissADME in silico analysis, all four dyes could be substrates of P-glycoprotein 1, which suggests a potential interaction with cell membrane transporters.[16] In contrast to Cy7, AF750 and IRDye750 contain multiple sulfonate groups, which make them negatively charged and increase their water solubility. DY-750 is a zwitterionic dye, which therefore has no net charge when used for labeling.

The content of the AEMA linkers in the pHPMA were determined using the trinitrobenzenesulfonic acid assay and

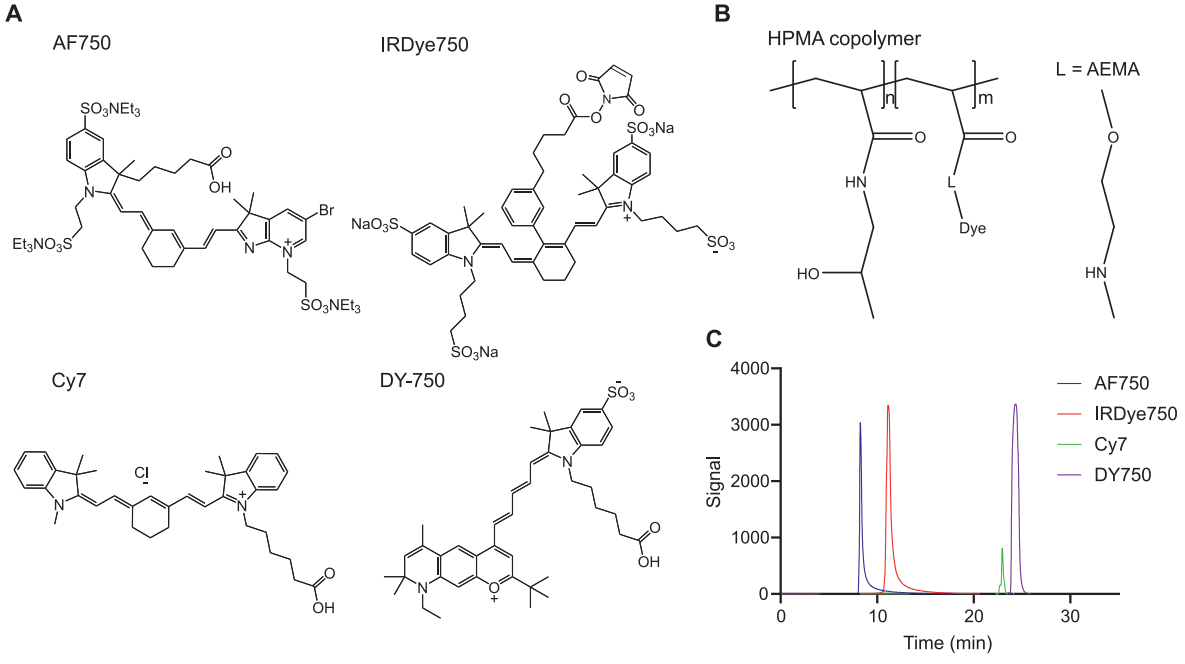

Fig. 1. NIRF dye structure and hydrophobicity. (A) Dye structure and (B) coupled to pHPMA. (C) Relative dye hydrophobicity.

found to be 6.3 mol% (Fig. 1B). Size exclusion chromatography showed the pHPMA polymer to have a molecular weight of 40 kDa and a dispersity of 1.07. For the dye-pHPMA conjugates, a dye amount of about 0.3 mol% was calculated according to the feed ratio during synthesis.

Dye and dye-pHPMA conjugate stability was tested via HPLC. AF750 and IRDye750 were stable for 144 h (Fig. S1). DY-750 was less stable than AF750 and IRDye750, degrading by 11.1 ± 2.5 % within 48 h. As free DY-750 was mostly eliminated from the body within 6 h this is anticipated to have little influence on the biodistribution. This contrasts with Cy7, which degraded by 68.7 ± 7.2 % within 48 h. Stability issues with cyanine dyes were previously reported for another cyanine dye in liposomes, but not or to a lesser extent for other fluorescent dyes.[17,18] Next, we investigated the stability of dyes on pHPMA and their dissociation (being indicated by a different retention time in HPLC). AF750-, IRDye750-, and Cy7-pHPMA conjugates were stable for 96 h. DY-750-pHPMA tended to degrade, however, after 96 h still 69.9 % remained stable. Considering elimination times we do not assume a major influence of dye degradation on our biodistribution results.

Cellular uptake of dyes and dye-pHPMA conjugates

Dye uptake was normalized by calibration curves. There were significant differences in the uptake by A431 squamous cell carcinoma cells (Fig. 2B). Cellular uptake was highest for DY-750, followed by Cy7 and IRDye750, and lowest for AF750. Dye uptake correlated with hydrophobicity r = 0.99 (Fig. 2C). For AF750 and IRDye750, there were no significant differences between the uptake at 37 °C and 4 °C, whereas the uptake of Cy7 and DY-750 was significantly reduced at 4 °C. For the latter, this indicates an active temperature-dependent transport, possibly via endocytosis or a membrane transporter.

In the context of transporter-mediated uptake, we next studied whether the uptake of dyes was OATP-mediated as indicated by the literature (e.g., OATPs were shown to play a role in the clearance of ICG by the liver)[14]. Therefore, we first investigated OATP expression in A431 cells. OATPs are cell membrane transporters found in various tissues and are involved in the uptake of endogenous substrates, as well as various drugs.[19] In A431 cells the expression of OATP1B3 was highest, as described before,[19] followed by OATP1A2 and OATP1B1. OATP2B1 expression could not be detected (Fig. 2A). Various OATP inhibitors were tested to block free dye uptake (Fig. S4A). However, no significant decrease in dye uptake was observed after OATP inhibition. Only 17β-estradiol tended to reduce the uptake of Cy7 and DY-750.

As it was our intention to study the impact of different dye tags on macromolecules, we labeled pHPMA with the four dyes, respectively. pHPMA was chosen as it is a highly hydrophilic medical polymer.[20] We observed changes in optical properties of the dyes after their conjugation to pHPMA (Fig. S2), which however have no significant influence on our experiments due to fluorescence normalization. Cellular uptake of the 40 kDa dye-pHPMA conjugates was lower than that of the free dyes, even at longer incubation times, presumably because macromolecules pass cell membranes and transporter channels less well (Fig. 2D). The uptake of DY-750-pHPMA was highest, followed by AF750-pHPMA, Cy7-pHPMA, and IRDye750-pHPMA. Except for AF750-pHPMA, the hydrophobicity of the dye label correlated with the degree of uptake. The high uptake of AF750-pHPMA was surprising, as AF750 is the most hydrophilic dye that did not undergo active uptake.

For all conjugates, there was no clear OATP-mediated transport, as their uptake was not clearly reduced by the classical OATP inhibitor rifampicin (Fig. S4B). There was a tendency of 17β-estradiol (which is partially internalized by OATPs) to reduce the uptake of all dye-pHPMAs, which, however, was only significant for the polymer labeled with the most hydrophobic dye (DY-750-pHPMA ($p < 0.05$)).

Biodistribution and pharmacokinetics of dyes differ substantially

NIRF dye biodistribution was studied in A431 tumor-bearing mice, which were injected with the fluorescent probe and

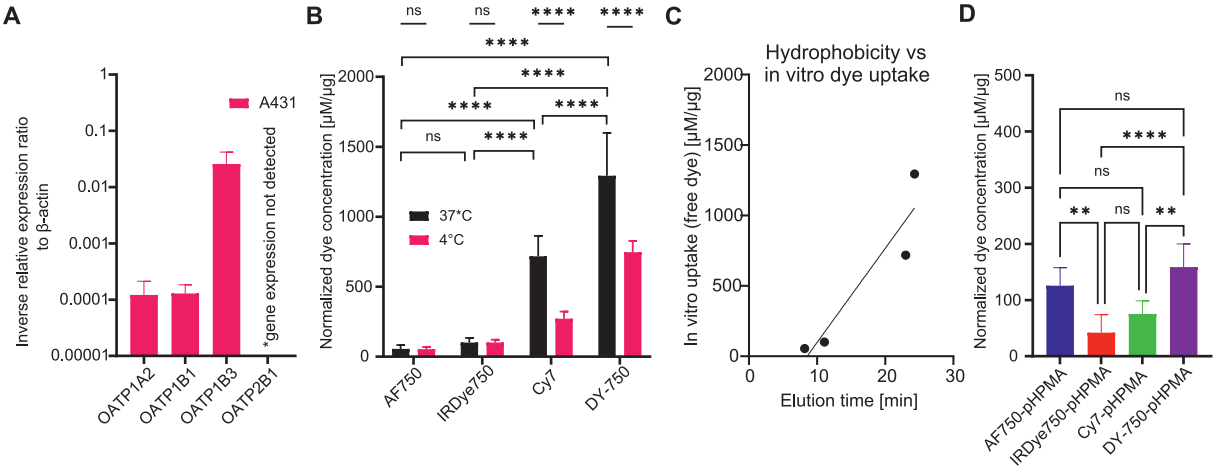

Fig. 2. In vitro uptake of NIRF dyes and dye-pHPMA conjugates. (A) Relative OATP expression in A431 cells ($n = 3$). (B) Dye uptake into A431 cells ($n = 6$). (C) Correlation of dye hydrophobicity and in vitro uptake. (D) Dye-pHPMA uptake ($n = 6$). One-way ANOVA with Holm-Šidák correction for multiple testing in B (lower statistic values) and D, two-way ANOVA with Šidák multiple comparison correction in B (upper statistic values). Data shown as mean ± SD.

subsequently imaged longitudinally by CT-FLT for five days (Fig. 3). Fluorescence signals were normalized based on the first injection.

Among the free dyes, biodistribution profiles differed significantly (see Fig. 4A–D for mean organ values and Fig. S5A–B for total organ and area under the curve (AUC) values). IRDye750 had the longest blood half-life (1.8 h), followed by Cy7 (1.3 h), DY-750 (1.2 h) and AF750 (0.1 h). IRDye750 predominantly showed hepatobiliary clearance (21.2 % injected dose (ID)/cm^3 and 7.2 % ID/cm^3 in liver and intestine at 0.25 h, respectively) but was also found in the bladder (25.7 % ID/cm^3 at 0.25 h) (Fig. S6), suggesting a mixed clearance. Its longer persistence in liver and intestine than the other dyes may be explained by a stronger enterohepatic recirculation. This process is commonly known for bile acids, but also for hormones and various drugs, for example estradiol.[21] Cy7 strongly accumulated in liver and intestine (28.4 % ID/cm^3 and 4.0 % ID/cm^3 at 0.25 h, respectively) indicating a mainly hepatobiliary clearance. DY-750 mostly accumulated in the liver (28.8 % ID/cm^3 at 0.25 h) but could not be prominently found in the intestine, kidneys, and bladder (2.6 % ID/cm^3, 1.8 % ID/cm^3, 0.2 % ID/cm^3 at 0.25 h, respectively). Thus, we assume hepatic degradation. AF750 was excreted by the kidneys as indicated by its rapid accumulation in the kidneys (18.4 % ID/cm^3 at 0.25 h) and the bladder (241 % ID/cm^3 at 0.25 h), respectively. As reported for other small molecule dyes, renal elimination decreased with increasing hydrophobicity.[22–24]

Free dye tumor uptake was highest for IRDye750 (3.1 % ID/cm^3 and 3.5 % ID/cm^3 at 0.25 h and 3 h, respectively), followed by Cy7 (2.4 % ID/cm^3 and 3.1 % ID/cm^3 at 0.25 h and 3 h, respectively), and lowest for AF750 (2.1 % ID/cm^3 and 0.0 % ID/cm^3 at 0.25 h and 3 h, respectively), and DY-750 (1.6 % ID/cm^3 and 0.4 % ID/cm^3 at 0.25 h and 3 h, respectively) (Fig. 4D). Here, tumor uptake did not correlate with hydrophobicity as for the in vitro results, but rather with blood half-lives.

Dye labels influence biodistribution of DDS

After assessing the biodistribution of the free dyes, the model DDS pHPMA was labeled with the dyes to investigate their impact on tumor cell uptake, biodistribution, and tumor accumulation.

The conjugates AF750-pHPMA and IRDye750-pHPMA (labeled with the most hydrophilic dyes) accumulated more in the kidneys and less in liver and intestine than Cy7-pHPMA and DY-750-pHPMA (see Fig. 5A–E for mean organ values and Fig. S5C–D for total organ and AUC values). All conjugates showed a mainly hepatobiliary clearance.

Blood half-lives of all dye-pHPMAs were over 6 h without significant differences among them (Fig. 5B). Thus, the blood half-lives of dye-pHPMAs are not strongly influenced by dye labeling and differences can be attributed to individual variations between mice, as well as to the methodology, which is less accurate than invasive blood sampling.

Tumor uptake differed among the conjugates (Fig. 5C). 24 h after injection, DY-750-pHPMA tumor concentration was the highest with 6.6 ± 1.1 % ID/cm^3, whereas tumor concentrations for Cy7- and AF750-pHPMA were 5.3 ± 0.9 % ID/cm^3 and 4.6 ± 0.7 % ID/cm^3, respectively. IRDye750-pHPMA had the lowest uptake with 2.2 ± 0.7 % ID/cm^3. Thus, the tumor uptake was three times higher for DY-750-pHPMA than for IRDye750-pHPMA. Interestingly, the tumor uptake of the dye-pHPMAs in vivo was in line with the obtained in vitro results on A431 cells (Fig. 5D). Cellular uptake in vitro and tumor uptake in vivo at 3 h and 24 h correlated positively with r = 0.99 ($p < 0.05$) and r = 0.84 ($p = 0.16$), respectively. At 96 h, tumor concentrations had decreased for all conjugates, which was most pronounced for IRDye750-pHPMA.

Ex vivo analysis confirms dye-labeling bias

After 96 h, mice were euthanized, and organs were excised to perform optical reflectance imaging analysis. Organs of mice

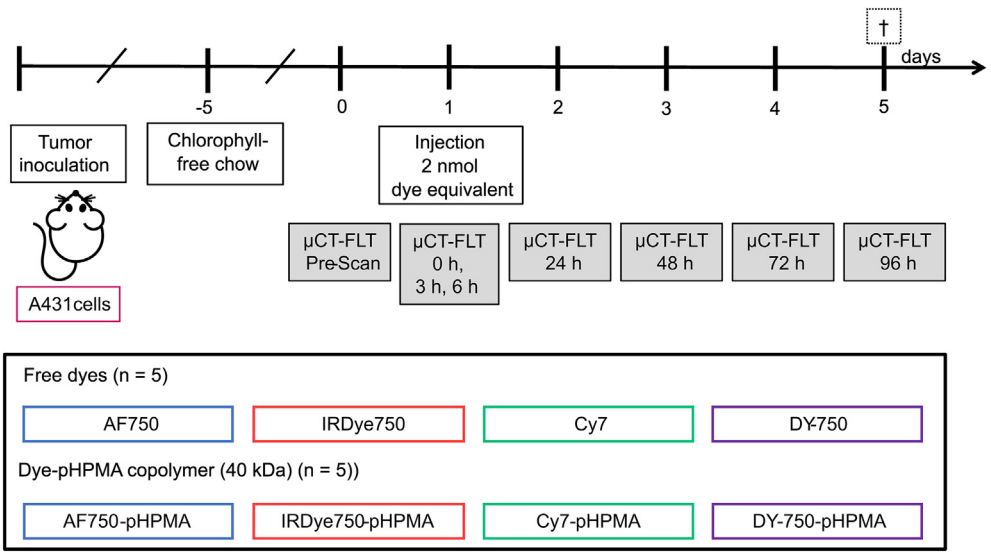

Fig. 3. In vivo study design. A431 tumor-bearing mice were imaged longitudinally for 96 h after injection of dye or dye-pHPMA.

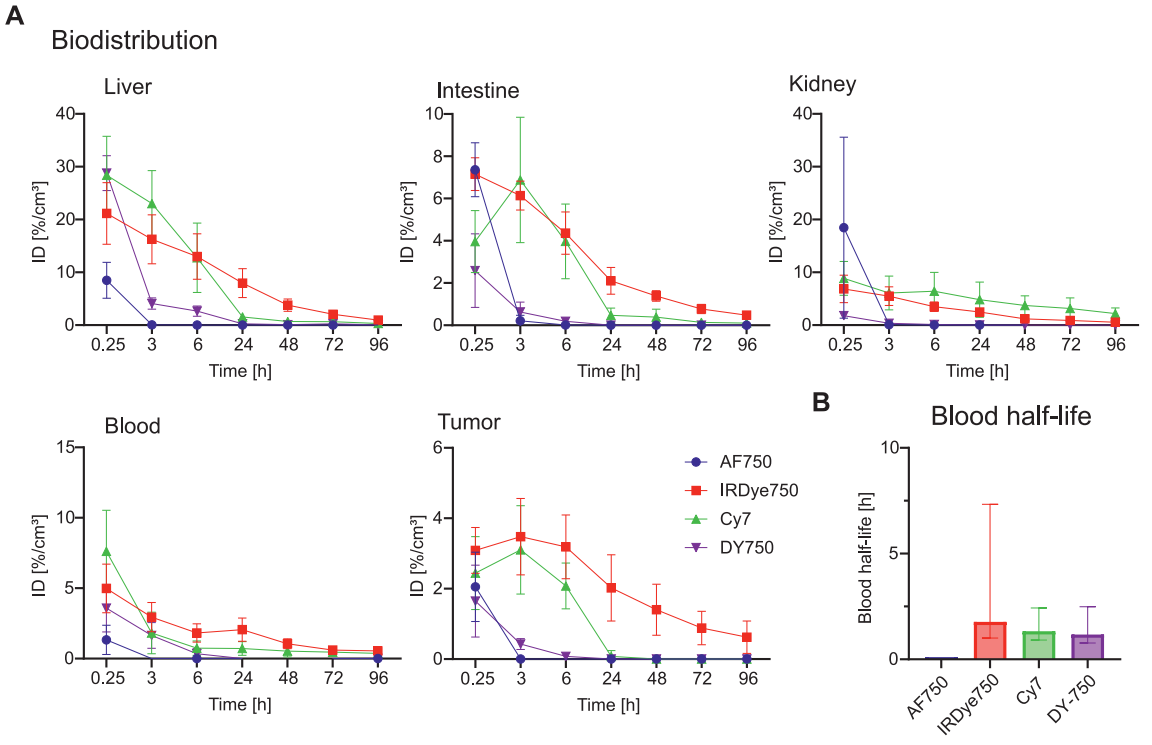
A
Biodistribution
Liver
Intestine
Kidney
Blood
Tumor
ID [%/cm³]
Time [h]
0.25
3
6
24
48
72
96
AF750
IRDye750
Cy7
DY750
B
Blood half-life
Blood half-life [h]

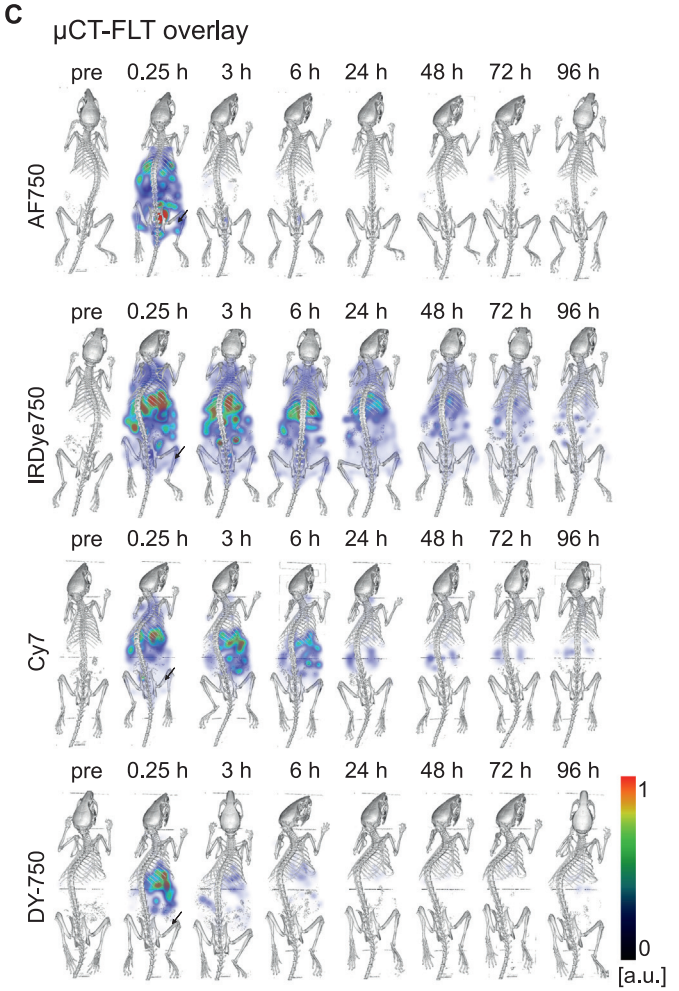
C
µCT-FLT overlay
pre
0.25 h
3 h
6 h
24 h
48 h
72 h
96 h
AF750
IRDye750
Cy7
DY-750
1
0
[a.u.]

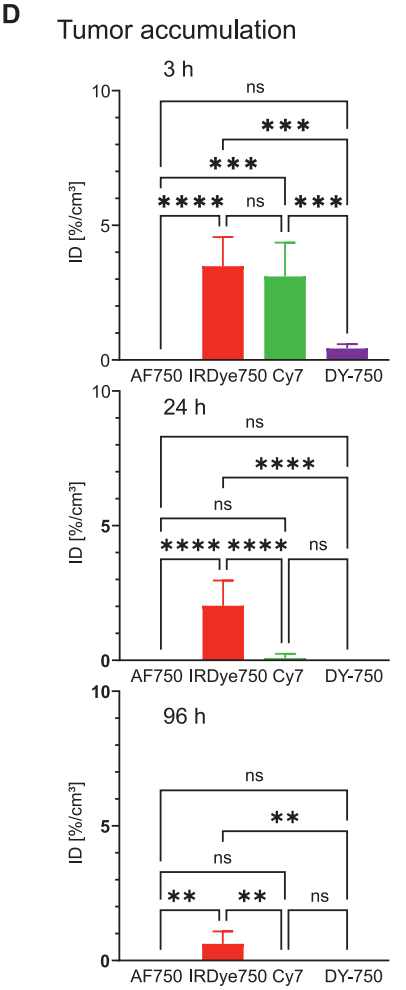
D
Tumor accumulation
3 h
24 h
96 h
ID [%/cm³]
ns
***
****
**
AF750
IRDye750
Cy7
DY-750

injected with free dyes no longer showed significant fluorescence (data not shown). This is in line with our finding that the free dyes have short half-lives and are cleared rapidly from the body.

High kidney accumulation of AF750-pHPMA and IRDye750-pHPMA as well as the relatively high liver accumulation of Cy7-pHPMA and DY-750-pHPMA could be confirmed (Fig. 5F–G) by the ex vivo analyses. Furthermore, the tumor accumulation assessed by in vivo and ex vivo analyses correlated positively with a Pearson correlation coefficient of r = 0.66 (data not shown).

Optical reflectance imaging yields raw fluorescence signals. Due to the differing fluorescence brightness, comparing the different dye-pHPMAs is imprecise in this setting. Thus, we focused on relative differences in organ accumulation. Tumor accumulation patterns can only be compared with caution.

Discussion

In this paper, we investigated how NIRF dye labels influence pharmacokinetics and biodistribution of macromolecules. This has not been systematically evaluated yet, but is of high importance for all scientists using optical imaging tags in drug development and biodistribution studies to avoid bias deriving from the label. So far, there are only limited studies on the influence of the dye structure on physicochemical properties, plasma protein binding or pharmacokinetics.[22,23,25] None of these studies compared different dyes as a label.

To understand the general behavior of different dyes, we first investigated their stability, hydrophobicity, cellular uptake, pharmacokinetics, and biodistribution. Stability of dye-pHPMA conjugates and free dyes was similar, except for Cy7-pHPMA. There, the stability of the conjugate was higher than that of the free dye, which could be due to steric stabilization by the polymer, as has been described, for example, for nanoparticles or polymer-prodrug systems.[26–28]

Hydrophobicity and net charges of the dyes differed substantially. The investigated dyes have one positive charge at the conjugated fluorophore system, and up to four sulfonate anions. Charges are known to play a role in the internalization of polymeric particles.[29,30] Because the dyes had varying chemical properties, we expected them to be distributed, metabolized, and excreted differently. For instance, more hydrophobic compounds can cross cell membranes more easily.[31] Thus, it was not surprising that the hydrophobic dyes showed higher tumor cell internalization in vitro than the hydrophilic ones. A second determinant of dye internalization might be transporter-mediated uptake. Temperature-dependent uptake of Cy7 and DY-750, indicated transporter- or endocytosis-mediated uptake. For example, ICG is known to be taken up by OATP1B3.[14,32] However, the dyes examined in this study were not taken up actively by OATPs, as competitive blocking various OATPs did not markedly decrease their internalization. This contrasts with previous reports about other fluorescent dyes.[32–37] These studies might not be representative for clinical tumor situations as they were all performed on pharmacologically stimulated or genetically transformed cells overexpressing OATPs. Nevertheless, there is evidence that also natural cell lines with divergent OATP profiles internalize dyes via OATPs, specifically IR-780, IR-783, and MHI-148.[35–37] The low OATP-mediated transport in our study may be due to the fact that first, A431 cells are not expressing OATPs to the same extent, and second, other transporters besides OATPs might play a role in the internalization of dyes. For example, 17β-estradiol showed a trend toward inhibiting uptake of the dyes, probably because it has further internalizing mechanisms that may also be relevant for the dyes.[38] It is a substrate of other members of the solute carrier transporter family, such as organic cation transporters.[39,40] Thus, these influx transporters might also play a role in the dye uptake. Independent of the uptake of 17β-estradiol, P2X receptors might be involved in the uptake of dyes since they were previously found to mediate uptake of cationic dyes.[41] Here, extensive in vitro studies are needed to gain further insights into influx and efflux transporters carrying fluorescent dyes.

The different blood half-lives of the dyes studied might have multiple reasons: It is known that some more hydrophobic dyes bind to plasma proteins and only unbound fractions can undergo renal or hepatobiliary clearance.[22,42–44] Plasma protein binding can extend dyes' blood half-life. Presuming that the most hydrophilic dye tested had the lowest albumin binding, it was not surprising that AF750 had the shortest blood half-life. Furthermore, it was cleared renally, which is faster than hepatobiliary clearance. Here, in addition to passive glomerular filtration, active secretion into renal tubules may also be involved, as all dyes studied are likely to be substrates of P-glycoprotein 1 (Table S1).[45,46]

Liver uptake is another determinant of blood half-life. When the dye is internalized by hepatocytes, it can be metabolized by phase I or phase II enzymes to become more hydrophilic and/or transported to the bile by various transporters, among others P-glycoprotein 1.[45,47] DY-750, the most hydrophobic dye, is metabolized rapidly by the liver decreasing the time to accumulate in tumors and other organs. For Cy7 and IRDye750, we observed the longest blood half-lives, blood AUCs, and tumor accumulation. Here, albumin binding is likely. Previous research has already shown that binding of certain cyanine dyes to albumin prolonged their circulation time,[25,44,48] and albumin accumulates in tumors via the enhanced permeability and retention (EPR) effect.[49,50] Thus, the blood half-life and biodistribution depend on the interplay of renal elimination, (transporter-mediated) hepatobiliary clearance and binding to plasma proteins but not directly on the hydrophobicity of the dye.

After studying the free dyes, we evaluated their function as imaging tags. For this purpose, pHPMA was used as a model DDS.[27] It is a highly biocompatible polymer that accumulates in

Fig. 4. Biodistribution of NIRF dyes. (A) Dye distribution in organs differ significantly ($n = 5$). (B) Blood half-lives were 0.1 h (1.00; 1.00), 1.8 h (0.99; 0.63), 1.2 h (0.99; 0.83), and 1.3 h (1.00; 0.78) for AF750, IRDye750, Cy7, and DY-750 respectively (in brackets: corresponding coefficients of determination for the non-linear fit and the linear regression). (C) Examples of 3D CT-FLT overlay for dyes. Tumor location indicated by arrows. (D) Tumor accumulation of dyes at 3 h, 24 h, and 96 h, respectively ($n = 5$). One-way ANOVA with Holm-Šidák correction for multiple testing in D ($n = 5$). Data shown as mean ± SD. ID: injected dose.

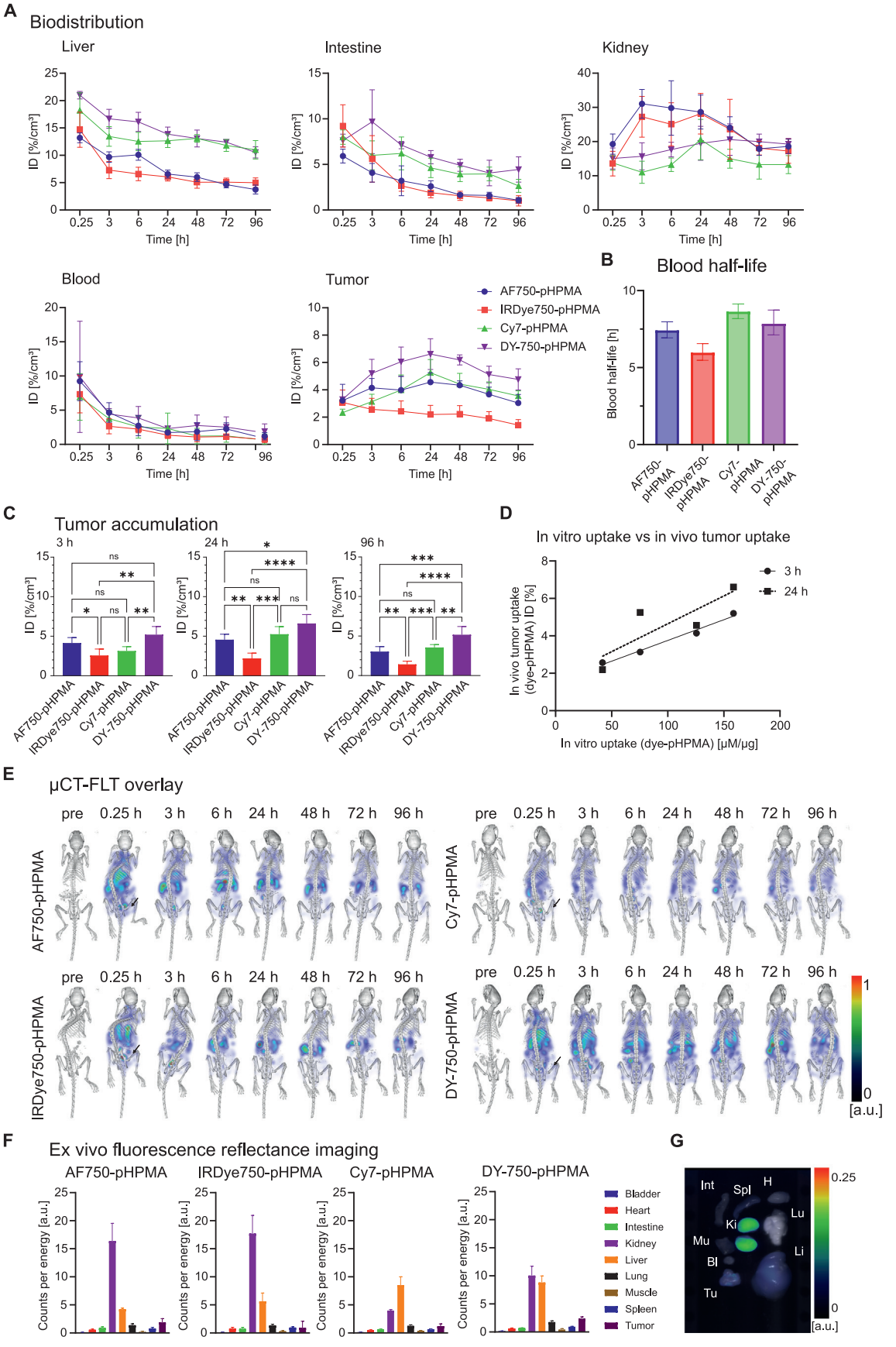
A
Biodistribution
Liver
Intestine
Kidney
Blood
Tumor
ID [%/cm³]
Time [h]
AF750-pHPMA
IRDye750-pHPMA
Cy7-pHPMA
DY-750-pHPMA
B
Blood half-life
Blood half-life [h]
C
Tumor accumulation
3 h
24 h
96 h
D
In vitro uptake vs in vivo tumor uptake
In vivo tumor uptake (dye-pHPMA) ID [%]
In vitro uptake (dye-pHPMA) [µM/µg]
E
µCT-FLT overlay
pre
0.25 h
3 h
6 h
24 h
48 h
72 h
96 h
[a.u.]
F
Ex vivo fluorescence reflectance imaging
Counts per energy [a.u.]
Bladder
Heart
Intestine
Kidney
Liver
Lung
Muscle
Spleen
Tumor
G
Int
Spl
H
Lu
Ki
Mu
Li
Bl
Tu
[a.u.]

tumors due to the EPR effect but shows no particular cell receptor affinity due to its non-fouling properties.[49–51]

Cellular uptake of the dye-pHPMAs was lower than free dyes' uptake and largely followed their hydrophobicity. We hypothesize that hydrophobic dyes could become an affinity anchor for the hydrophilic polymer chains. An exception was AF750-pHPMA, the conjugate labeled with the most hydrophilic dye, showing comparable intracellular concentrations as DY-750-pHPMA, the conjugate labeled with the most hydrophobic dye. The increased uptake of dye-pHPMAs might be of therapeutic benefit and used for a theranostic approach. However, for this purpose, in-depth exploration of the mechanism is required, especially for AF750-pHPMA, where increased uptake cannot be explained by its hydrophobicity. Seeking for an explanation for the unexpectedly high uptake of AF750-pHPMA, transporter-mediated uptake was studied. It is unlikely that the 40 kDa sized dye-pHPMA conjugates pass the cell membrane through influx transporters, as the usual substrate size of OATPs is not larger than 1 kDa.[45] As the original pHPMA is internalized by fluid-phase endocytosis,[52,53] internalization of the entire OATP-conjugate complex is most likely.[54] Competitive blocking experiments with the OATP inhibitors rifampicin and 17β-estradiol were performed. Rifampicin could not inhibit the internalization of the conjugates, but there was a trend for 17β-estradiol to reduce dye-pHPMA conjugates' uptake. However, as this was least strong for AF750-pHPMA, OATP-mediated uptake is not the main reason for its strong uptake. Eventually, the charge of the dyes influenced the size and shape of the random coil of the pHPMA,[12] leading to different compactness of the systems and thus diverging cellular uptake. Multiply negatively charged dye tags might lead to both higher cellular binding and higher background signal in different organs than dye labels with balanced charges.[12] As AF750 has three negative charges, the altered 3D structure of pHPMA might trigger cellular uptake. Secondly, AF750 is the only dye containing a halogen atom, which increases fluorescence lifetime and electronegativity.[55] Previous research showed that introduction of a halogen atom increases cellular uptake.[56] Thus, AF750 might adsorb to the cell membrane, but is only endocytosed conjugated to pHPMA. In addition, AF750-pHPMA might form a receptor ligand, leading to an increased endocytosis- or receptor-triggered cell uptake.

In vivo, availability from the blood is the main prerequisite for tissue uptake. Thus, blood half-life was the major determinant for free dyes' accumulation in tumors. In contrast, all dye-pHPMA conjugates showed similarly long blood half-lives. Also, strong accumulation in tumors was described before.[57–59] However, there were significant differences in tumor uptake depending on the dye, although only 0.3 mol% dye/pHPMA, approximately one dye per polymer chain, were used. The results on tumor accumulation in vivo were in line with the results obtained on tumor cells in vitro (including the surprisingly high uptake of AF750-pHPMA). Dye labeling also influenced the biodistribution of pHPMA. For example, liver accumulation was higher for the conjugates with the more hydrophobic labels, i.e., Cy7-pHPMA and DY-750-pHPMA, whereas kidney accumulation was higher for the conjugates with a more hydrophilic dye label. Here, in addition to the increased hydrophobicity, self-assemblies, detected by dynamic light scattering measurements (Fig. S3), could further increase the uptake of Cy7-pHPMA and DY-750-pHPMA into the liver.

Translating dye labeling effects to other probe classes is difficult, and further systematic labeling studies with biomolecules such as antibodies are needed for the research community. Nevertheless, it is evident that there is an influence of dye labeling on biodistribution and tumor accumulation, which has also been observed, e.g., using labeled antibody formats.[5] Here, Hage et al. compared AF750- (FLT) with ^{64}Cu-NODAGA-labeling (PET) and found that dye labeling led to increased liver and tumor uptake in comparison to radiolabeling. However, the actual biodistribution without any labeling was not determined. In our case, this would have been complex. The detection of unlabeled pHPMA would require extensive ex vivo studies, e.g., using hybrid mass spectrometry microscopy,[60] or radiochemical synthesis involving incorporation of ^{14}C into the pHPMA in combination with microautoradiography. In addition, the assessment of the natural distribution of pHPMA was not the scope of this article. This manuscript intended to highlight the importance of understanding the interactions of NIRF dyes with biomolecules to avoid wrong conclusions on therapeutic efficacy, adverse effects, and toxicity.

In conclusion, labeling of nanocarriers like pHPMA with only approximately one dye molecule per polymer significantly impacts biodistribution and tumor uptake. This is related to complex multifactorial processes including dye stability, hydrophobicity, cell membrane interaction, receptor binding, and protein binding affinity of the dye tags. Although we could identify active uptake for two of the dyes, we could not confirm a prominent involvement of OATPs, which contrasts with reports on other dyes and cell lines.[32–37] Thus, this study highlights the need for considering potential bioeffects of imaging tags, which are not restricted to optical labels and that need to be further investigated. If neglected, false conclusions on the function, biodistribution, and performance of nanocarriers or biomolecules may be the consequence.

As a practical recommendation, our results qualify AF750 and IRDye750 for labeling hydrophilic nanocarriers due to their hydrophilicity, high stability, and low active cellular uptake.

Fig. 5. In vivo and ex vivo biodistribution of dye-pHPMA conjugates. (A) Dye-pHPMA distribution among liver, intestine, kidney, blood, and tumor differs significantly ($n = 5$ per group and $n = 4$ for DY-750-pHPMA). (B) Blood half-lives of dye-pHPMA conjugates (corresponding coefficients of determination for the non-linear fit and the linear regression were 0.79 and 0.99, 0.78 and 0.98, 0.56 and 0.99, and 0.44 and 0.98 for AF750-pHPMA, IRDye750-pHPMA, Cy7-pHPMA, and DY-750-pHPMA, respectively). (C) Tumor accumulation of dye-pHPMA conjugates at 3 h, 24 h and 96 h, respectively ($n = 5$, $n = 3$ for DY-750-pHPMA). (D) In vitro uptake and in vivo uptake correlation at 3 h and 24 h, respectively. (E) Examples of 3D CT-FLT overlay for dye-pHPMAs. Tumor location indicated by arrows. (F) Ex vivo 2D fluorescence reflectance imaging shows total organ fluorescence of excised organs. Signal is expressed in counts per energy. (G) Ex vivo organ scan with reflectance overlay, exemplary for DY-750-pHPMA. One-way ANOVA with Holm-Šidák correction for multiple testing in D ($n = 5$ per group and $n = 3$ for DY-750-pHPMA). Data shown as mean ± SD. Bl: bladder; H: heart; ID: injected dose; Int: intestine; Ki: kidneys; Li: liver; Lu: lung; Mu: muscle; Spl: spleen; Tu: tumor.

CRediT authorship contribution statement

Sarah Schraven: Methodology, Investigation, Writing - Original draft preparation **Stefanie Rosenhain**: Conceptualization, Methodology, Investigation, Funding acquisition, Reviewing **Ramona Brueck**: Investigation, Reviewing **Tim Marvin Wiechmann**: Investigation, Reviewing **Robert Pola**: Investigation, Reviewing **Tomas Etrych**: Funding acquisition, Supervision, Reviewing **Wiltrud Lederle**: Funding acquisition, Supervision, Reviewing **Twan Lammers**: Supervision, Reviewing **Felix Gremse**: Conceptualization, Funding acquisition, Supervision, Reviewing **Fabian Kiessling**: Conceptualization, Funding acquisition, Supervision, Reviewing.

Declaration of competing interest

FG is the owner of Gremse-IT. SR is employed at Gremse-IT.

Acknowledgements

The authors thank Quim Peña for HPLC method development.

Appendix A. Supplementary data

Supplementary data to this article can be found online at https://doi.org/10.1016/j.nano.2023.102650.

References

1. Arakawa R, Takano A, Halldin C. PET technology for drug development in psychiatry. *Neuropsychopharmacol Rep* 2020;**40**:114-21.
2. Waaijer SJH, Kok IC, Eisses B, Schröder CP, Jalving M, Brouwers AH, et al. Molecular imaging in cancer drug development. *J Nucl Med* 2018; **59**:726-32.
3. Gremse F, Theek B, Kunjachan S, Lederle W, Pardo A, Barth S, et al. Absorption reconstruction improves biodistribution assessment of fluorescent nanoprobes using hybrid fluorescence-mediated tomography. *Theranostics* 2014;**4**:960-71.
4. Ntziachristos V, Ripoll J, Wang LV, Weissleder R. Looking and listening to light: the evolution of whole-body photonic imaging. *Nat Biotechnol* 2005;**23**:313-20.
5. Hage C, Gremse F, Griessinger CM, Maurer A, Hoffmann SHL, Osl F, et al. Comparison of the accuracy of FMT/CT and PET/MRI for the assessment of antibody biodistribution in squamous cell carcinoma xenografts. *J Nucl Med* 2018;**59**:44-50.
6. Rosenhain S, Al Rawashdeh W, Kiessling F, Gremse F. Sensitivity and accuracy of hybrid fluorescence-mediated tomography in deep tissue regions. *J Biophoton* 2017;**10**:1208-16.
7. Álamo P, Pallarès V, Céspedes MV, Falgàs A, Sanchez JM, Serna N, et al. Fluorescent dye labeling changes the biodistribution of tumor-targeted nanoparticles. *Pharmaceutics* 2020;**12**:1004.
8. Gupta P, Wentland J-A, Leal M, Ma D, Roach R, Esparza A, et al. Assessment of near-infrared fluorophores to study the biodistribution and tumor targeting of an IL13 receptor α2 antibody by fluorescence molecular tomography. *Oncotarget* 2017;**8**:57231-45.
9. Debie P, Van Quathem J, Hansen I, Bala G, Massa S, Devoogdt N, et al. Effect of dye and conjugation chemistry on the biodistribution profile of near-infrared-labeled nanobodies as tracers for image-guided surgery. *Mol Pharm* 2017;**14**:1145-53.
10. Kalliokoski A, Niemi M. Impact of OATP transporters on pharmacokinetics: OATP transporters and pharmacokinetics. *Br J Pharmacol* 2009;**158**:693-705.
11. Stieger B, Hagenbuch B. Organic anion-transporting polypeptides. In: Bevensee MO, editor. *Current Topics in Membranes*. Amsterdam: Elsevier; 2014. p. 205-32.
12. Choi HS, Gibbs SL, Lee JH, Kim SH, Ashitate Y, Liu F, et al. Targeted zwitterionic near-infrared fluorophores for improved optical imaging. *Nat Biotechnol* 2013;**31**:148-53.
13. Klohs J, Wunder A, Licha K. Near-infrared fluorescent probes for imaging vascular pathophysiology. *Basic Res Cardiol* 2008;**103**: 144-51.
14. Ho C-M, Dhawan A, Hughes RD, Lehec SC, Puppi J, Philippeos C, et al. Use of indocyanine green for functional assessment of human hepatocytes for transplantation. *Asian J Surg* 2012;**35**:9-15.
15. Gremse F, Stärk M, Ehling J, Menzel JR, Lammers T, Kiessling F. Imalytics preclinical: interactive analysis of biomedical volume data. *Theranostics* 2016;**6**:328-41.
16. Daina A, Michielin O, Zoete V. SwissADME: a free web tool to evaluate pharmacokinetics, drug-likeness and medicinal chemistry friendliness of small molecules. *Sci Rep* 2017;**7**:42717.
17. Cauzzo J, Nystad M, Holsæter AM, Basnet P, Škalko-Basnet N. Following the fate of dye-containing liposomes in vitro. *Int J Mol Sci* 2020;**21**:4847.
18. Creamer JS, Mora MF, Noell AC, Willis PA. Long-term thermal stability of fluorescent dye used for chiral amino acid analysis on future spaceflight missions. *Electrophoresis* 2019;**40**:3117-22.
19. Obaidat A, Roth M, Hagenbuch B. The expression and function of organic anion transporting polypeptides in Normal tissues and in cancer. *Annu Rev Pharmacol Toxicol* 2012;**52**:135-51.
20. Dozono H, Yanazume S, Nakamura H, Etrych T, Chytil P, Ulbrich K, et al. HPMA copolymer-conjugated pirarubicin in multimodal treatment of a patient with stage IV prostate cancer and extensive lung and bone metastases. *Targ Oncol* 2016;**11**:101-6.
21. Roberts MS, Magnusson BM, Burczynski FJ, Weiss M. Enterohepatic circulation: physiological, pharmacokinetic and clinical implications. *Clin Pharmacokinet* 2002;**41**:751-90.
22. Hamann FM, Brehm R, Pauli J, Grabolle M, Frank W, Kaiser WA, et al. Controlled modulation of serum protein binding and biodistribution of asymmetric cyanine dyes by variation of the number of sulfonate groups. *Mol Imaging* 2011;**10** 7290.2011.00005.
23. Press AT, Butans MJ, Haider TP, Weber C, Neugebauer S, Kiehntopf M, et al. Fast simultaneous assessment of renal and liver function using polymethine dyes in animal models of chronic and acute organ injury. *Sci Rep* 2017;**7**:15397.
24. Marshall MV, Draney D, Sevick-Muraca EM, Olive DM. Single-dose intravenous toxicity study of IRDye 800CW in Sprague-dawley rats. *Mol Imaging Biol* 2010;**12**:583-94.
25. Bai L, Hu Z, Han T, Wang Y, Xu J, Jiang G, et al. Super-stable cyanine@albumin fluorophore for enhanced NIR-II bioimaging. *Theranostics* 2022;**12**:4536-47.
26. Resch-Genger U, Grabolle M, Nitschke R, Nann T. Nanocrystals and nanoparticles versus molecular fluorescent labels as reporters for bioanalysis and the life sciences: a critical comparison. In: Demchenko AP, editor. *Advanced Fluorescence Reporters in Chemistry and Biology II Molecular Constructions, Polymers and Nanoparticles*. Berlin Heidelberg: Springer; 2010. p. 3-40.
27. Chytil P, Kostka L, Etrych T. HPMA copolymer-based nanomedicines in controlled drug delivery. *J Pers Med* 2021;**11**:115.
28. Chytil P, Kostka L, Etrych T. Structural design and synthesis of polymer prodrugs. In: Scholz C, editor. *Polymers for Biomedicine: Synthesis, Characterization, and Applications*. Hoboken, NJ: John Wiley & Sons, Inc.; 2017. p. 391-420.
29. Harush-Frenkel O, Rozentur E, Benita S, Altschuler Y. Surface charge of nanoparticles determines their endocytic and transcytotic pathway in polarized MDCK cells. *Biomacromolecules* 2008;**9**:435-43.
30. Abdel-Bar HM, Walters AA, Lim Y, Rouatbi N, Qin Y, Gheidari F, et al. An "eat me" combinatory nano-formulation for systemic immunotherapy of solid tumors. *Theranostics* 2021;**11**:8738-54.

31. Pires DEV, Blundell TL, Ascher DB. pkCSM: predicting small-molecule pharmacokinetic and toxicity properties using graph-based signatures. *J Med Chem* 2015;**58**:4066-72.
32. Nyström NN, Yip LCM, Carson JJL, Scholl TJ, Ronald JA. Development of a human photoacoustic imaging reporter gene using the clinical dye indocyanine green. *Radiol Imaging Cancer* 2019; **1**e190035.
33. Shi C, Wu JB, Chu GC-Y, Li Q, Zhang C, Zhang Y, et al. Heptamethine carbocyanine dye-mediated near-infrared imaging of canine and human cancers through the HIF-1α/ OATPs signaling axis. *Oncotarget* 2014;**5**:10114-26.
34. Lee Y-H, Wu M-R, Hsiao J-K. Organic anion transporting polypeptide 1B1 is a potential reporter for dual MR and optical imaging. *Int J Mol Sci* 2021;**22**:8797.
35. Wu JB, Shi C, Chu GC-Y, Xu Q, Zhang Y, Yu JS, et al. Near-infrared fluorescence heptamethine carbocyanine dyes mediate imaging and targeted drug delivery for human brain tumor. *Biomaterials* 2015; **67**:1-10.
36. Zhang E, Luo S, Tan X, Shi C. Mechanistic study of IR-780 dye as a potential tumor targeting and drug delivery agent. *Biomaterials* 2013; **35**:771-8.
37. Yuan J, Yi X, Yan F, Wang F, Qin W, Wu G, et al. Near-infrared fluorescence imaging of prostate cancer using heptamethine carbocyanine dyes. *Mol Med Rep* 2015;**11**:821-8.
38. Gui C, Miao Y, Thompson L, Wahlgren B, Mock M, Stieger B, et al. Effect of pregnane X receptor ligands on transport mediated by human OATP1B1 and OATP1B3. *Eur J Pharmacol* 2008;**584**:57-65.
39. Roth M, Obaidat A, Hagenbuch B. OATPs, OATs and OCTs: the organic anion and cation transporters of the SLCO and SLC22A gene superfamilies: OATPs, OATs and OCTs. *Br J Pharmacol* 2012;**165**: 1260-87.
40. Hayer-Zillgen M. Expression and pharmacological profile of the human organic cation transporters hOCT1, hOCT2 and hOCT3. *Br J Pharmacol* 2002;**136**:829-36.
41. Chaïb N, Kabré E, Alzola E, Pochet S, Dehaye JP. Bromoenol lactone enhances the permeabilization of rat submandibular acinar cells by P2X 7 agonists: P2X 7 receptors in salivary glands. *Br J Pharmacol* 2000;**129**:703-8.
42. Al-Husseini JK, Stanton NJ, Selassie CRD, Johal MS. The binding of drug molecules to serum albumin: the effect of drug hydrophobicity on binding strength and protein desolvation. *Langmuir* 2019;**35**:17054-60.
43. Roberts JA, Pea F, Lipman J. The clinical relevance of plasma protein binding changes. *Clin Pharmacokinet* 2013;**52**:1-8.
44. Tian R, Zeng Q, Zhu S, Lau J, Chandra S, Ertsey R, et al. Albumin-chaperoned cyanine dye yields superbright NIR-II fluorophore with enhanced pharmacokinetics. *Sci Adv* 2019;**5**eaaw0672.
45. Giacomini KM, Huang S-M, Tweedie DJ, Benet LZ, Brouwer KLR, Chu X, et al. Membrane transporters in drug development. *Nat Rev Drug Discov* 2010;**9**:215-36.
46. Varma MVS, Feng B, Obach RS, Troutman MD, Chupka J, Miller HR, et al. Physicochemical determinants of human renal clearance. *J Med Chem* 2009;**52**:4844-52.
47. Sevior DK, Pelkonen O, Ahokas JT. Hepatocytes: the powerhouse of biotransformation. *Int J Biochem Cell Biol* 2012;**44**:257-61.
48. Tian R, Feng X, Wei L, Dai D, Ma Y, Pan H, et al. A genetic engineering strategy for editing near-infrared-II fluorophores. *Nat Commun* 2022;**13**:2853.
49. Matsumura Y, Maeda H. A new concept for macromolecular therapeutics in cancer chemotherapy: mechanism of tumoritropic accumulation of proteins and the antitumor agent smancs. *Cancer Res* 1986; **46**:6387.
50. Maeda H. Tumor-selective delivery of macromolecular drugs via the EPR effect: background and future prospects. *Bioconjug Chem* 2010; **21**:797-802.
51. Klepac D, Kostková H, Petrova S, Chytil P, Etrych T, Kereïche S, et al. Interaction of spin-labeled HPMA-based nanoparticles with human blood plasma proteins – the introduction of protein-corona-free polymer nanomedicine. *Nanoscale* 2018;**10**:6194-204.
52. Hovorka O, Etrych T, Šubr V, Strohalm J, Ulbrich K, Říhová B. HPMA based macromolecular therapeutics: internalization, intracellular pathway and cell death depend on the character of covalent bond between the drug and the peptidic spacer and also on spacer composition. *J Drug Target* 2006;**14**:391-403.
53. Liu J, Bauer H, Callahan J, Kopečková P, Pan H, Kopeček J. Endocytic uptake of a large array of HPMA copolymers: elucidation into the dependence on the physicochemical characteristics. *J Control Release* 2010;**143**:71-9.
54. Hong M, Hong W, Ni C, Huang J, Zhou C. Protein kinase C affects the internalization and recycling of organic anion transporting polypeptide 1B1. *Biochim Biophys Acta* 2015;**1848**:2022-30.
55. Amiot C, Xu S, Liang S, Pan L, Zhao J. Near-infrared fluorescent materials for sensing of biological targets. *Sensors* 2008;**8**:3082-105.
56. Ungati H, Govindaraj V, Mugesh G. The remarkable effect of halogen substitution on the membrane transport of fluorescent molecules in living cells. *Angew Chem Int Ed Engl* 2018;**57**:8989-93.
57. Noguchi Y, Wu J, Duncan R, Strohalm J, Ulbrich K, Akaike T, et al. Early phase tumor accumulation of macromolecules: a great difference in clearance rate between tumor and Normal tissues. *Jpn J Cancer Res* 1998;**89**:307-14.
58. Wang D, Sima M, Mosley RL, Davda JP, Tietze N, Miller SC, et al. Pharmacokinetic and biodistribution studies of a bone-targeting drug delivery system based on N -(2-Hydroxypropyl)methacrylamide copolymers. *Mol Pharm* 2006;**3**:717-25.
59. TGGM Lammers. *Drug Targeting to Tumors Using HPMA Copolymers*; 2009.
60. Buchberger AR, DeLaney K, Johnson J, Li L. Mass spectrometry imaging: a review of emerging advancements and future insights. *Anal Chem* 2018;**90**:240-65.